

# Cross-correlation between WMAP and 2MASS: non-Gaussianity induced by SZ effect

Liang Cao<sup>1,2\*</sup> Yao-Quan Chu<sup>1,3</sup> and Li-Zhi Fang<sup>4</sup>

<sup>1</sup>Center for Astrophysics, University of Science and Technology of China, Hefei, Anhui 230026, China

<sup>2</sup>Institute of Modern Physics, Chinese Academy of Science, Lanzhou, Gansu, 730000, China

<sup>3</sup>National Astronomical Observatories, Chinese Academy of Science, Beijing 100012, China

<sup>4</sup>Department of Physics, University of Arizona, Tucson, AZ 85721

17 August 2018

## ABSTRACT

We study the SZ-effect-induced non-Gaussianity in the cosmic microwave background (CMB) fluctuation maps. If a CMB map is contaminated by the SZ effect of galaxies or galaxy clusters, the CMB maps should have similar non-Gaussian features as the galaxy and cluster fields. Using the WMAP data and 2MASS galaxy catalog we show that the non-Gaussianity of the 2MASS galaxies is imprinted on WMAP maps. The signature of non-Gaussianity can be seen with the 4<sup>th</sup> order cross correlation between the wavelet variables of the WMAP maps and 2MASS clusters. The intensity of the 4<sup>th</sup> order non-Gaussian features is found to be consistent with the contamination of the SZ effect of 2MASS galaxies. We also show that this non-Gaussianity can not be seen by the high order auto-correlation of the WMAP. This is because the SZ signals in the auto-correlations of the WMAP data generally is weaker than the WMAP-2MASS cross correlations by a factor  $f^2$ , which is the ratio between the powers of SZ effect map and the CMB fluctuations on the scale considered. Therefore, the ratio of high order auto-correlations of CMB maps to cross-correlations of the CMB maps and galaxy field would be effective to constrain the powers of SZ effect on various scales.

**Key words:** cosmology: theory - large-scale structure of the universe

## 1 INTRODUCTION

The thermal Sunyaev-Zel'dovich (SZ) effect, or the inverse-Compton scattering of the cosmic microwave background (CMB) photons by hot electrons, shifts the spectrum of the CMB photons to higher energy when the photons pass through the regions of cosmic hot gas. It yields a CMB temperature  $T$  change at frequency  $\nu$  given by

$$\frac{\Delta T_{\text{sz}}(\mathbf{n})}{T} = y(\mathbf{n}) \left( x \frac{e^x + 1}{e^x - 1} - 4 \right), \quad (1)$$

where the dimensionless Compton  $y$ -parameter is

$$y(\mathbf{n}) = \sigma_T \int dl \frac{n_e k(T_e - T)}{m_e c^2}, \quad (2)$$

where the integral is along the line of sight of  $\mathbf{n}$ , and  $\mathbf{n} = (l, b)$ ,  $b$  being the Galactic latitude and  $l$  the Galactic longitude.  $\sigma_T$  is the cross section of the Thomson scattering and  $x = h\nu/kT$ .  $n_e$  and  $T_e$  are, respectively, the number density and temperature of hot electrons. Since groups and clusters of galaxies are hosts of hot gas and their distributions are non-Gaussian, the SZ effect will imprint

the non-Gaussianity of groups and clusters on the maps of the CMB temperature fluctuations (Cole & Kaiser 1988).

Since the WMAP data became available (Bennett et al 2003a, 2003b), many groups have detected the SZ effect signals with the cross-correlation between WMAP data and galaxy samples. The X-ray based catalogues of clusters and galaxies, including the Northern ROSAT All Sky Galaxy Cluster Survey (Böhringer et al. 2000) and the ROSAT Brightest Cluster Sample (Ebeling et al. 1998) are found to be cross-correlated with the WMAP maps at the 2-5  $\sigma$  level (Hernández-Monteagudo and Rubiño-Martín 2004). The samples of groups and clusters identified from the APM galaxy survey (Maddox et al. 1990), and 2MASS (Jarrett et al. 2000) show cross correlation with  $W$  band data of the WMAP (Myers et al. 2004). The WMAP-2MASS correlation is also found by comparing it with model expectation (Afshordi et al. 2004). Using a semi-analytic model of the Intra-Cluster Medium, SZ signal was detected from 116 low redshift X-ray clusters at  $\sim 8\sigma$  level (Afshordi et al. 2005).

On the other hand, the WMAP data are found to be Gaussian, especially no significant non-Gaussian signals have been detected on scales of clusters (e.g. Komatsu et al. 2003). Therefore, a problem is whether the positive results of detecting the SZ effect with WMAP-galaxy cross-correlation is consistent with the negative re-

\* E-mail:caoliang@mail.ustc.edu.cn

sults of detecting non-Gaussian features of the WMAP data alone? In this paper, we try to reconcile the two results. That is, we want to show that 1.) the WMAP maps contain SZ-effect-induced non-Gaussianity; 2.) this non-Gaussian signal cannot be seen with the WMAP maps alone.

We will study the non-Gaussianity induced by the SZ effect of the galaxy sample listed in the 2MASS extended source catalog. First, the SZ effects of 2MASS galaxies have been detected at about  $3\sigma$  level with the cross-correlation between the maps of WMAP and 2MASS (Myers et al. 2004; Afshordi et al. 2004). Second, the non-Gaussian features of the 2MASS samples have been extensively analyzed (Guo et al. 2004). It would be helpful to search for the WMAP's non-Gaussianity induced by the SZ effect of 2MASS galaxies.

The paper is organized as follows. In §2 we present the data used for the cross correlation analysis. §3 analyzes the SZ effects of the DWT clusters, which are identified from the 2MASS galaxies with the discrete wavelet transfer (DWT) decomposition. The non-Gaussianity of WMAP induced by the SZ effect of the 2MASS DWT clusters is analyzed in §4. The discussion and conclusion are given in §5. Some math stuffs with the DWT algorithm are given in Appendix.

## 2 SAMPLES AND ITS DWT DESCRIPTION

### 2.1 Data of CMB temperature fluctuations

We use the foreground cleaned WMAP maps,  $\Delta T(\mathbf{n})$ , of  $W$  and  $Q$  bands (Bennett et al. 2003a). The contamination of the galactic foreground is reduced by mask  $Kp2$  (Bennett et al. 2003b). These maps were used for producing the WMAP first-year power spectrum of CMB temperature fluctuations. The foreground signal, consisting of synchrotron, free-free, and dust emission have been removed.

The frequency of  $Q$  band is 40.7 GHz, and the SZ effect is  $(\Delta T_{sz}/T)_Q = -1.91y$ , while the frequency of  $W$  band is 93.6 GHz, we have  $(\Delta T_{sz}/T)_W = -1.56y$ . That is, at these two frequencies, the SZ signals  $\Delta T_{sz}$  is less than 0. Therefore, the SZ signals would be survived during the removal of foreground *emission* sources.

### 2.2 2MASS-XSC galaxies

We use the 2MASS extended source catalog (XSC, Jarrett et al. 2000), which covers almost the entire sky at wavelength between 1 and 2  $\mu\text{m}$ . The condition of selecting galaxies is taken to be  $K_{\text{m},\text{k20fe}}$ , which measures the magnitude inside a elliptical isophote with surface brightness of 20 mag  $\text{arcsec}^{-2}$  in  $K_s$ -band. There are approximately 1.6 million extended objects with  $K_s < 14.3$ . Most of the XSC sources at  $|b| > 20^\circ$  are galaxies ( $> 98\%$ ). The contamination mainly is from stars. The reliability of separating stars from extended sources is 95% at  $|b| > 10^\circ$ , but drops rapidly to  $< 65\%$  at  $|b| > 5^\circ$ . To avoid the contaminant of stars, we use a latitude cut of  $|b| > 10^\circ$ . We also removed a small number of bright ( $K_s < 9$ ) sources by the parameters of the XSC confusion flag (cc\_flag) and visual verification score for source (vc). They are identified as non-extended sources including artifacts. Moreover, to eliminate duplicate sources and have a uni-

form sample, we use the following parameters: use\_src = 1 and dup\_src = 0<sup>1</sup>.

To select the range of  $K_s$ , we use the standard  $\log N - \log S$  test to examine the completeness of the sample. The number counts can be approximated by a power-law (Afshordi et al. 2004) as

$$\frac{dN}{dm} \propto 10^{\kappa m}. \quad (3)$$

The XSC sources with  $|b| > 30^\circ$  and  $12 < K_s < 13.7$  are believed to be galaxies with 99% reliability (McIntosh et al. 2003). For this sample, the index  $\kappa$  is found to be  $0.641 \pm 0.006$ . If considering this  $\kappa$  to be the standard, the completeness of a sample can be estimated by the deviation of  $(dN/dm)_{\text{sample}}$  from the standard, i.e.

$$C(m) = \frac{(dN/dm)_{\text{standard}}}{(dN/dm)_{\text{sample}}}, \quad (4)$$

where the standard sample is taken to  $12 < K_s < 13.7$  and  $|b| > 30^\circ$ . It has been shown by Guo et al. (2004) that the completeness  $C(m)$  is equal to 1 for sample of  $|b| > 10^\circ$  in the range  $11 < K_s < 13.7$ . The factor  $C(m)$  is obviously larger than 1 for sample of  $|b| > 30^\circ$  when  $K_s < 10.0$ . This indicates the catalog to be contaminated towards the bright end. On the other hand,  $C(m)$  drops below 0.9 when  $K_s > 14.0$ . Thus we use a cut of  $10.0 < K_s < 14.0$  to ensure our sample to be complete greater than 90%. This sample contains 987,125 galaxies with median redshift  $z \sim 0.1$ . It gives a 2-D number density field of galaxies,  $\rho_g(\mathbf{n})$ .

### 2.3 DWT variables of maps

To analyze the cross correlation and non-Gaussian signals, we will use the variable given by the discrete wavelet analysis (DWT) decomposition. That is, statistical properties are measured by DWT mode-mode correlation, and non-Gaussianity is detected by high order statistics of the DWT variables. Since the DWT mode is localized in phase (position and scale) space, and has regular shape, it can also be used for 1.) handle the bad pixels in maps; 2.) identify clusters from galaxy map.

Since the SZ effect is on small scales, one can subject the CMB temperature maps to an equal-area projection by the Lambert azimuthal algorithm:

$$\begin{aligned} x_1 &= R\sqrt{2 - 2|\sin b|} \cos l, \\ x_2 &= R\sqrt{2 - 2|\sin b|} \sin l, \end{aligned} \quad (5)$$

where  $R$  is a relative scale factor,  $b$  is the Galactic latitude and  $l$  is the Galactic longitude. This hemisphere scheme projects the whole sky into two circular plane, northern and southern sky. 2MASS galaxies are also described by this format. We select a square with  $123^\circ.88 \times 123^\circ.88$  in the central part of each circular plane. We have two fields of  $123^\circ.88 \times 123^\circ.88$  in northern and southern sky. Both the WMAP map and 2MASS galaxy distribution are fully overlapped with each other. We will use coordinate  $\mathbf{x} = (x_1, x_2)$  to replace  $\mathbf{n} = (l, b)$  below. The 2-D maps of  $\Delta T(\mathbf{n})$  and  $\rho_g(\mathbf{n})$  will be written as  $\Delta T(\mathbf{x})$  and  $\rho_g(\mathbf{x})$ .

The DWT variables are defined as

$$\Delta T_{j,1} = \frac{1}{\int \phi_{j,1}(\mathbf{x}) d\mathbf{x}} \int \Delta T(\mathbf{x}) \phi_{j,1}(\mathbf{x}) d\mathbf{x}, \quad (6)$$

<sup>1</sup> The notations of the 2MASS parameters used in this paragraph are from the list shown in the 2MASS Web site <http://www.ipac.caltech.edu/2mass/releases/allsky/doc>.

$$\rho_{j,1} = \frac{1}{\int \phi_{j,1}(\mathbf{x}) d\mathbf{x}} \int \rho_g(\mathbf{x}) \phi_{j,1}(\mathbf{x}) d\mathbf{x},$$

and

$$\begin{aligned} \tilde{\epsilon}_{j,1}^T &= \int \Delta T(\mathbf{x}) \psi_{j,1}(\mathbf{x}) d\mathbf{x}, \\ \tilde{\epsilon}_{j,1}^g &= \int \rho_g(\mathbf{x}) \psi_{j,1}(\mathbf{x}) d\mathbf{x}, \end{aligned} \quad (7)$$

where  $\phi_{j,1}(\mathbf{x})$  and  $\psi_{j,1}(\mathbf{x})$  are, respectively, the scaling function and wavelet. For our 2-D samples, the DWT variables  $\Delta T_{j,1}$  and  $\rho_{j,1}$  describe, respectively, the mean temperature and the mean number density of galaxies in the cell  $(\mathbf{j}, \mathbf{l})$ , which has size  $123^\circ.88/2^{j_1} \times 123^\circ.88/2^{j_2}$  and at position around  $[l_1(123^\circ.88)/2^{j_1}, l_2(123^\circ.88)/2^{j_2}]$ , where  $j_1$  and  $j_2$  can be any integral, and  $l_1 = 0, \dots, 2^{j_1-1}$ ,  $l_2 = 0, \dots, 2^{j_2-1}$ . Thus, the DWT index  $j$  corresponds to an angular scale of  $123^\circ.88/2^j$ . The angular distance between modes  $\mathbf{l}$  and  $\mathbf{l}'$  at scale  $j$  is given by  $\theta = 123.88^\circ |\mathbf{l} - \mathbf{l}'|/2^j$ . The wavelet variables (WFCs)  $\tilde{\epsilon}_{j,1}^T$  and  $\tilde{\epsilon}_{j,1}^g$  describe, respectively, the fluctuations of temperature and galaxy density on scale  $j$  and position  $\mathbf{l}$ . Some details of the algorithm with the DWT is given in Appendix A.

The 2MASS XSC galaxies are resolved to  $10''$ . Our analysis of the 2MASS sample can reach to angular scale of about 0.01 degree. However, on scales less than  $\theta = 123^\circ.88/2^9 = 0^\circ.24$ , the WMAP data are dominated by noise. In calculating the WMAP-2MASS cross correlation or WMAP's auto-correlation, we will use only scales of  $j = 8$ .

Since the DWT variable  $\Delta T_{j,1}$  is localized, it can be used to handle the foreground masks. A standard technique to treat contaminated pixels is zero-padding (Pando & Fang 1998). That is, 1.) put zero data at the masked pixels, and 2.) off-count the DWT modes  $(\mathbf{j}, \mathbf{l})$  located at the masked pixels. We test the zero padding by simulation samples generated with code HEALPix<sup>2</sup>. The results show the  $Kp2$  masked samples with zero padding yield the same statistical properties as the original simulated samples, at least, up to the 4<sup>th</sup> order.

We should emphasize that the Lambert projection will violate the rotational invariance on the spherical surface. We will not use the rotational invariance in our analysis. Moreover, we show in Appendix B that the Lambert projection does not cause false non-Gaussian features. That is, if the original map is free from non-Gaussian correlations, the projected map is also free from these correlations. The Lambert projection is legitimate for our DWT analysis.

### 3 THE SZ EFFECT OF 2MASS CLUSTERS

#### 3.1 DWT clusters of 2MASS galaxies

The SZ effect is sensitive to hot gas clouds. If the mass density and temperature of gas are proportional to the number density of galaxies, one can identify hot gas clouds on scale  $\mathbf{j}$  by modes  $(\mathbf{j}, \mathbf{l})$  with the high  $\rho_{j,1}$ . These modes  $(\mathbf{j}, \mathbf{l})$  are called DWT clusters on scale  $\mathbf{j}$ . The general method of identifying DWT clusters with  $\rho_{j,1}$  have been studied with simulation and real samples (Xu et al. 1999, 2000). It showed that the clusters identified by top  $\rho_{j,1}$  statistically are the same as the clusters identified by the friend-of-friend

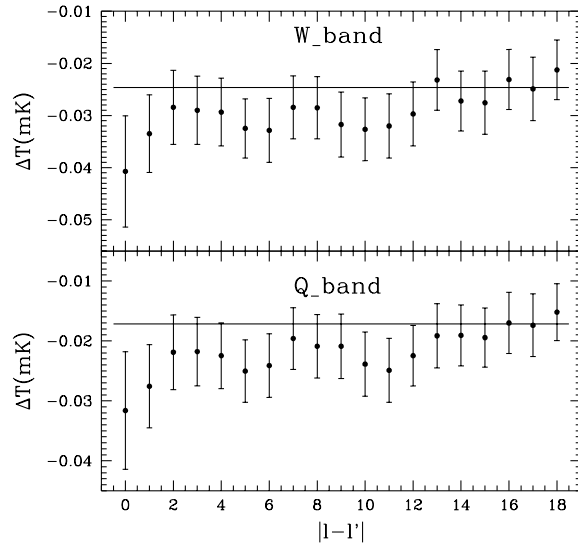


**Figure 1.** Cross correlation  $\langle T(|l - l'|) \rangle$  [eq.(8)] between the WMAP maps of  $W$  (top) and  $Q$  (bottom) bands and top 500 2MASS DWT clusters on scale  $j = 8$ . The angular scale of  $|l - l'|$  is  $|l - l'|123.88/2^8$  degree.

method if the mean size of the friend-of-friend identified clusters is the same as that of DWT clusters.

The scale of DWT variables is well defined, and therefore, it is parameter-free. On the other hand, the friend-of-friend algorithm needs the so-called link parameter. These parameters may introduce uncertainty in the correlation analysis. Moreover, The clusters identified by the friend-of-friend method usually have very irregular shapes (Jing & Fang 1994), it is inconvenient to estimate the statistical significance of the cross correlation between CMB maps and galaxy catalog. On the other hand, the variables  $\rho_{j,1}$  and  $\Delta T_{j,1}$  are in the same spatial cell of DWT mode, the statistical significance with  $\rho_{j,1}$  and  $\Delta T_{j,1}$  is unambiguous. The DWT scaling functions are orthogonal from each other, different DWT clusters consist of different galaxies. This is also useful for statistical analysis.

We identified, in this paper, the DWT clusters on  $j = 8$ , which corresponds to angular scale  $123^\circ.88/2^8 \simeq 0^\circ.5$ , or length scale  $\simeq 1.8 \text{ h}^{-1} \text{ Mpc}$  at the median redshift of the sample, which is the scale of clusters of galaxies. We selected 500 cells with top  $\rho_{j,1}$ , which are the peaks with  $6.4\sigma$  and higher,  $\sigma$  being the variance of the fluctuations of the number density field of galaxies. The number of galaxies in the top 500 cells is from about 20 to 60. Although the 500 cells is identified with 2-D sample, they most likely contain projected clusters or groups.

#### 3.2 The contamination of SZ effect

We perform the cross-correlation between the WMAP data and the 2MASS DWT clusters by

$$\Delta T(|l - l'|) = \langle C_{j,1} \Delta T_{j,1} \rangle, \quad (8)$$

where the variable  $C_{j,1}$  is taken to be 1 for mode  $(\mathbf{j}, \mathbf{l})$  corresponding to a DWT cluster on scale  $j = 8$ , and  $C_{j,1} = 0$ , other modes. The average  $\langle \dots \rangle$  overs all possible  $|l - l'|$  of the sample. Therefore,  $\Delta T(|l - l'|)$  is an average CMB temperature fluctuations with a distance  $|l - l'|$  from DWT clusters on scale  $j = 8$ .

<sup>2</sup> The Healpix homepage: <http://www.eso.org/science/healpix>

## 4 Cao, Chu & Fang

Figure 1 presents the cross correlation  $\Delta T(|l - l'|)$  of  $W$  and  $Q$  band maps with the top 500 2MASS DWT clusters. For each DWT cluster, one can have a correlation  $\Delta T(|l - l'|)$ . The solid line and error bar in each panel of Fig. 1 are, respectively, given by the average and  $1-\sigma$  variance of  $\Delta T(|l - l'|)$  of the considered 500 top DWT clusters. Figure 1 shows anti-correlation of the DWT clusters with  $\Delta T$  at  $|l - l'| = 0$  with temperature decrease  $\Delta T_{sz} \equiv \Delta T(|l - l'|) - \langle \Delta T \rangle \simeq -15 \pm 10 \mu\text{K}$ , or the Compton  $y$ -parameter to be  $\simeq (3.7 \pm 2.4) \times 10^{-6}$ . This result is about the same as that given by 500 2MASS galaxy clusters selected by friends-of-friends algorithm (Myers et al. 2004). The frequency-dependence  $|\langle \Delta T_{sz}/T \rangle_Q| = 1.91y > |\langle \Delta T_{sz}/T \rangle_W| = 1.56y$  didn't shown in Figure 1. It is probably because the difference between  $\langle \Delta T_{sz}/T \rangle_Q$  and  $\langle \Delta T_{sz}/T \rangle_W$  is much less than the errors of Figure 1.

We also can see from Figure 1 that for  $Q$  band also have a weak anti-correlation at  $|l - l'| = 1$  with the level of  $\Delta T_{sz} \simeq -10 \pm 7 \mu\text{K}$ . This result indicates that the distribution of hot gas probably is not simply proportional to the number density of optical and infrared galaxies, but is more spread than the distribution of galaxies. Recently, cosmological hydrodynamic simulation shows indeed that the hottest gas generally distributes more spread than galaxies (He et al. 2005). Therefore, it would be reasonable to consider that hot gas is spread in the range of  $|l - l'| \leq 1$  around a DWT clusters.

We did not found significant anti-correlation with the DWT clusters more than top 500, or on scales larger than  $j = 8$ . Therefore, the 500 top DWT clusters give an estimation of the contamination on the WMAP maps induced by the SZ effect of 2MASS galaxies. On scale of  $j = 8$ , the map has divided into  $2 \times 256^2$  cells. The 500  $j = 8$  DWT clusters do not overlapped from each other, and therefore, there are about  $500/(2 \times 256^2) = 0.4\%$  area of the temperature maps of the WMAP to be contaminated by the 2MASS SZ effects with the order of  $\Delta T_{sz} \simeq -15 \pm 10 \mu\text{K}$ . Considering the  $Q$  band signal at  $|l - l'| = 1$ , the contaminated area would be about 1%.

### 3.3 Mock samples of SZ contaminated CMB maps

If the anti-correlation shown in Fig. 1 is due to the SZ effect of 2MASS clusters, we can mimic a SZ-effect-contaminated CMB map by the following mock sample

$$\Delta T(\mathbf{x}) = \Delta T_{\text{cmb}}(\mathbf{x}) + \Delta T_{\text{sz}}(\mathbf{x}) + \Delta T_{\text{second}}(\mathbf{x}), \quad (9)$$

where  $\Delta T_{\text{cmb}}(\mathbf{n})$  is the primeval temperature fluctuations, and  $\Delta T_{\text{second}}(\mathbf{n})$  is due to secondary effects other than the SZ effect, such as the ISW effect and microwave point sources. The term  $\Delta T_{\text{sz}}(\mathbf{x})$  of eq.(9) is given by eqs.(1) and (2). We consider only the SZ effects caused by hot electron in 2MASS galaxies, which are in a small redshift bin around  $z \simeq 0.1$ , it is described by surface density  $\rho_g(\mathbf{x})$ . Therefore, we rewrite the Compton parameter as  $y \simeq (\sigma_T/m_ec^2)n_e^{\text{col}}(\mathbf{n})T_e(\mathbf{n})$ , where  $n_e^{\text{col}}(\mathbf{n})$  is the column density of electrons, and  $T_e(\mathbf{n})$  is the density-weighted mean of temperature of electrons in the redshift range of 2MASS. Generally  $T_e \gg T_{\text{cmb}}$ . Therefore, the thermal SZ effect can be estimated as  $\Delta T_{\text{sz}}(\mathbf{x}) \propto n_e^{\text{col}}(\mathbf{x})T(\mathbf{x})$ .

If galaxies trace hot baryon gas, we have approximately  $n_e^{\text{col}}(\mathbf{x}) \propto \rho_g(\mathbf{x})$ . The relation between temperature  $T$  and mass density  $\rho_g$  actually is complicated, because the cosmic baryon gas is multiple phased (e.g. He et al. 2004). For a given dark matter (or baryon matter) mass density, the PDF (probability distribution function) of the temperature of baryon gas covers a large range

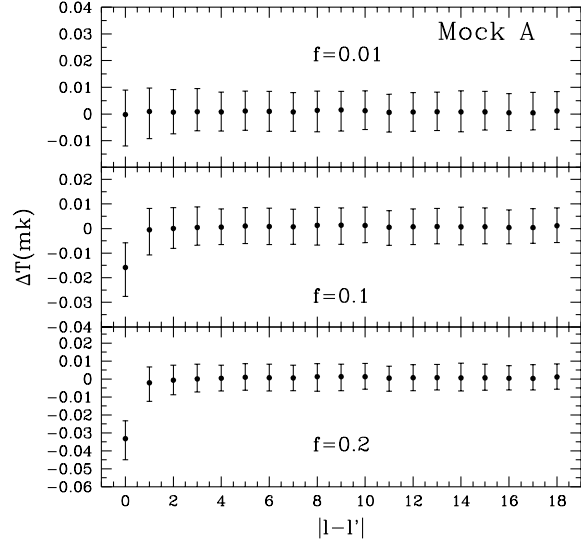


**Figure 2.** Cross correlation  $\langle \Delta T(|l - l'|) \rangle$  [eq.(8)] between mock sample A and top 500 2MASS DWT clusters on scale  $j = 8$ . The angular scale of  $|l - l'|$  is  $|l - l'|123.88/2^8$  degree.

from  $10^4$  to  $10^{6-7}$  K. Nevertheless, the relation between the mean temperature and mass density of the gas can be approximated as a polytropic relation  $T_e \propto \rho_g^{\alpha-1}$ , where  $\alpha$  is about 1.5 (He et al. 2004). Thus, we have  $\Delta T_{\text{sz}}(\mathbf{x}) \propto \rho_g^\alpha(\mathbf{x})$ . Therefore, to mimic the thermal SZ effect, it would be reasonable to assume

$$\Delta T_{\text{sz}}(\mathbf{x}) = -f \frac{\langle (\tilde{\epsilon}_{j,1}^T)^2 \rangle^{1/2}}{\langle (\tilde{\epsilon}_{j,1}^{g\alpha})^2 \rangle^{1/2}} \rho_g^\alpha(\mathbf{x}), \quad (10)$$

where  $\tilde{\epsilon}_{j,1}^T$  and  $\tilde{\epsilon}_{j,1}^{g\alpha}$  are, respectively, the wavelet variables (WFCs) of  $\Delta T_{\text{cmb}}(\mathbf{x})$  and  $\rho_g^\alpha(\mathbf{x})$  [eq.(7)]. Subjecting eq.(10) to a wavelet transform [eq.(7)], and considering  $\Delta T \gg \Delta T_{\text{sz}}, \Delta T_{\text{second}}$ , we have

$$f = \langle (\tilde{\epsilon}_{j,1}^{g\alpha})^2 \rangle^{1/2} / \langle (\tilde{\epsilon}_{j,1}^T)^2 \rangle^{1/2}. \quad (11)$$

Because  $\langle (\tilde{\epsilon}_{j,1}^T)^2 \rangle^{1/2}$  and  $\langle (\tilde{\epsilon}_{j,1}^{g\alpha})^2 \rangle^{1/2}$  are, respectively, the powers of the fields of CMB temperature fluctuations and SZ effect on scale  $j$  (Fang & Feng 2000), the parameter  $f$  is the ratio between the two powers on scale  $j$ .

Thus, with eq.(9) we can construct mock sample of SZ-effect-contaminated CMB maps by the following steps. First, the term  $\Delta T_{\text{cmb}}(\mathbf{x})$  in eq.(9) is produced by the HEALPix simulation. Second, the term  $\Delta T_{\text{sz}}(\mathbf{x})$  is given by eq.(10), in which  $\rho(\mathbf{x})$  is taken to be the value given by the 2MASS map if the position  $\mathbf{x}$  is within the cells of the top 500 clusters, otherwise,  $\rho_g(\mathbf{x})$  is taken to be equal to zero. We ignore the term  $\Delta T_{\text{second}}(\mathbf{x})$ . Finally, we estimate  $f$  by doing cross correlation between the mock sample eq.(9) and 2MASS DWT clusters. Figure 2 plots  $\Delta T(|l - l'|)$  vs.  $|l - l'|$  for  $f = 0.01, 0.1$  and  $0.2$ . The best fitting to the observed SZ temperature change  $\Delta T_{sz} \simeq -15 \pm 10 \mu\text{K}$  is given by  $f \simeq 0.1$ , which is ratio of the powers of SZ effect to the CMB fluctuations. This result is consistent with the estimation given by semi-analytical model and simulation (e.g. Cooray et al. 2004). This sample is called Mock A.

Unlike Figure 1, Figure 2 does not show the tail of  $\Delta T(|l - l'|)$  at  $|l - l'| \simeq 1$ . This is because we assume  $n_e(\mathbf{x}) \propto \rho_g(\mathbf{x})$ , i.e. no hot gas locates out side of a DWT cluster. If we assume that hot electron  $n_e(\mathbf{x})$  can exist not only at the cells of DWT clusters, but

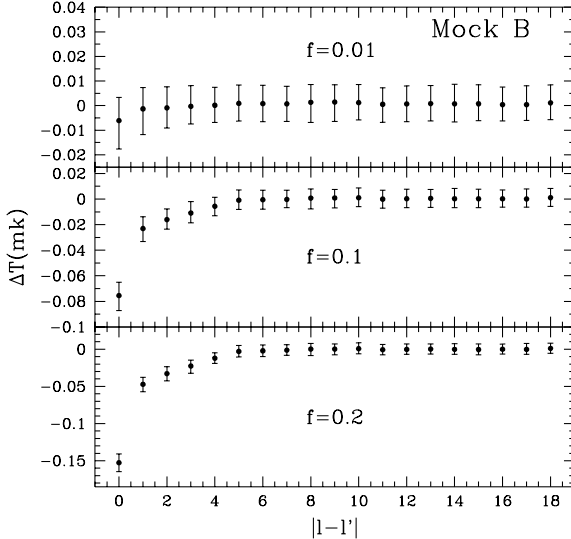


**Figure 3.** Cross correlation  $\langle T(|l - l'|) \rangle$  [eq.(8)] between mock sample B and top 500 2MASS DWT clusters on scale  $j = 8$ . The angular scale of  $|l - l'|$  is  $|l - l'|123.88/2^8$  degree.

also in their nearby cells, we have sample of Mock B. The cross correlation between mock sample B and 2MASS DWT clusters are shown in Fig.3, which does show a tail of  $\Delta T(|l - l'|)$ . We see that the sample of  $f = 0.1$  is also basically the same as observation.

The term  $\Delta T_{\text{second}}(\mathbf{x})$  of eq.(9) comes from the ISW and microwave point sources. The ISW effect is mainly from potential with linear evolution. The ISW effect given by nonlinear evolution is very small (Seljak 1996; Tuluie et al. 1996). One can ignore this effect if we focus on non-Gaussian behavior. If a microwave point source is from the 2MASS galaxies, their contributions to the SZ effect have already been included in the WMAP-2MASS cross correlation. If the microwave sources are not from the 2MASS galaxies, they generally are uncorrelated with 2MASS distribution  $\rho_g(\mathbf{x})$ , and therefore, the SZ signal of the 2MASS-WMAP cross correlation would not be hurt by this sources.

#### 4 NON-GAUSSIANITY INDUCED BY SZ EFFECT OF 2MASS GALAXIES

##### 4.1 Non-Gaussianity detectors

Using the mock samples, we try to estimate which non-Gaussian features are detectable with the WMAP samples. Effective detectors of non-Gaussianity are given by high order auto-correlations and cross-correlations of wavelet variables (WFCs)  $\Delta T_{\text{cmb}}(\mathbf{x})$  and  $\rho_g^\alpha(\mathbf{x})$  (e.g. Pando et al. 1998, 2002; Guo et al. 2004; McEwen et al. 2004; Cruz et al. 2005). The normalized high order correlation of wavelet variables is defined as

$$C_j^{p,q}(|l - l'|) \equiv \frac{\langle (\tilde{A}_{j,l})^p (\tilde{B}_{j,l'})^q \rangle}{\langle (\tilde{A}_{j,l})^p \rangle \langle (\tilde{B}_{j,l'})^q \rangle}, \quad (12)$$

where  $\tilde{A}_{j,l}$  and  $\tilde{B}_{j,l'}$  can be  $\tilde{\epsilon}_{j,l}^T$  or  $\tilde{\epsilon}_{j,l}^g$ . Because  $\langle \tilde{\epsilon}_{j,l}^T \rangle = \langle \tilde{\epsilon}_{j,l}^g \rangle = 0$ , the number  $p$  and  $q$  of eq.(12) should be even integer. When  $\tilde{A}_{j,l} = \tilde{B}_{j,l}$ ,  $C_j^{2,2}(0)$  is the kurtosis of the field considered. Therefore for a Gaussian field, we have

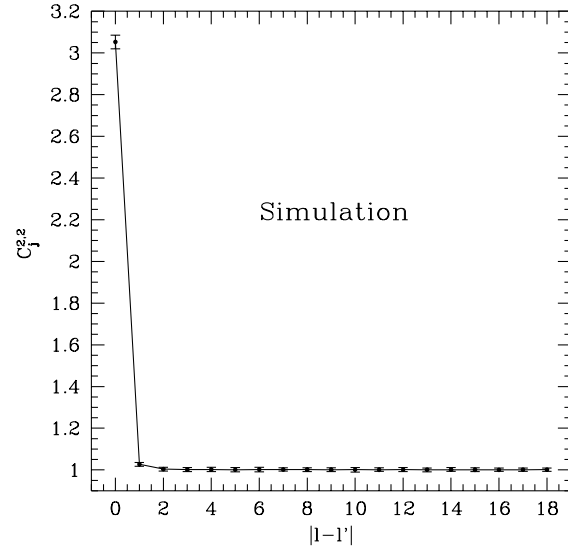


**Figure 4.**  $C_j^{2,2}(|l - l'|)$ , vs  $|l - l'|$  at  $\mathbf{j} = (j, j) = (8, 8)$  for CMB simulation samples. The error bars are the range of 90% of 100 samples.

$$C_j^{2,2}(|l - l'|) = \begin{cases} 3 & |l - l'| = 0 \\ 1 & |l - l'| > 0 \end{cases} \quad (13)$$

In Figure 4, we plots  $C_j^{2,2}(|l - l'|)$  for CMB map  $\Delta T_{\text{cmb}}(\mathbf{x})$  produced by the HEALPix simulation. As expected, this sample is Gaussian.

On the other hand, the sample of 2MASS-XSC galaxies is non-Gaussian (Guo et al. 2004). Figure 5 plots the  $|l - l'|$ -dependence of  $C_j^{2,2}(|l - l'|)$  for the 2MASS galaxies. We see that  $C_j^{2,2}(0)$  is significantly larger than 3, while at all other points, i.e.  $|l - l'| \neq 0$ , we have  $C_j^{2,2}(|l - l'|) = 1$ . That is, the non-Gaussianity of 2MASS samples measured by  $C_j^{2,2}(|l - l'|)$  is localized. It depends only on the density distribution of galaxies in the area considered, regardless galaxies in other places. With this feature, one can say that the mock sample eq.(10) contains all the 2MASS non-Gaussian features if they are measured by detectors eq.(12). Of course, if consider the contribution of hot electron in nearby areas of DWT clusters, like in mock sample B, the detector  $C_j^{2,2}(|l - l'|)$  would also show a tail till to about  $|l - l'| = 1$ . However, the non-Gaussianity measured by  $C_j^{2,2}(|l - l'|)$  still is localized in the sense that the hot electron distribution is determined by the position of the DWT clusters considered, regardless galaxies in other area.

##### 4.2 Signature of non-Gaussianity induced by SZ effect

To detect the WMAP non-Gaussianity given by SZ contamination of 2MASS galaxies, we use the 4<sup>th</sup> order cross-correlation between the CMB maps and 2MASS galaxy distribution defined as

$$C_j^{2,2}(|l - l'|)_{\text{cross}} = \frac{\langle (\tilde{\epsilon}_{j,l}^T)^2 (\tilde{\epsilon}_{j,l'}^g)^2 \rangle}{\langle (\tilde{\epsilon}_{j,l}^T)^2 \rangle \langle (\tilde{\epsilon}_{j,l'}^g)^2 \rangle}, \quad (14)$$

Using eqs.(9) and (10), we have

$$C_j^{2,2}(|l - l'|)_{\text{cross}} = \quad (15)$$

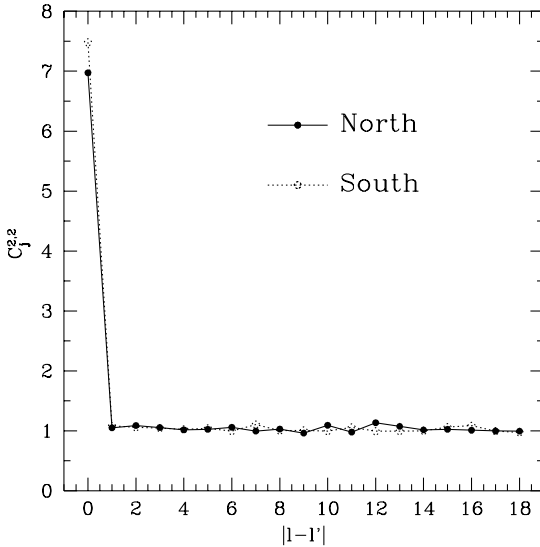


**Figure 5.**  $C_j^{2,2}(|l - l'|)$ , vs  $|l - l'|$  at  $j = (j, j) = (8, 8)$  for 2MASS galaxy samples of north (solid) and south (dashed).

$$\frac{\langle (\tilde{\epsilon}_{j,1}^T)^2 (\tilde{\epsilon}_{j,1'}^g)^2 \rangle}{\langle (\tilde{\epsilon}_{j,1}^T)^2 \rangle \langle (\tilde{\epsilon}_{j,1'}^g)^2 \rangle} + f^2 \frac{\langle (\tilde{\epsilon}_{j,1}^{g\alpha})^2 (\tilde{\epsilon}_{j,1'}^g)^2 \rangle}{\langle (\tilde{\epsilon}_{j,1}^{g\alpha})^2 \rangle \langle (\tilde{\epsilon}_{j,1'}^g)^2 \rangle}$$

Since there is no correlation between primeval CMB map and galaxies, we have  $\langle (\tilde{\epsilon}_{j,1}^T)^2 (\tilde{\epsilon}_{j,1'}^g)^2 \rangle = \langle (\tilde{\epsilon}_{j,1}^T)^2 \rangle \langle (\tilde{\epsilon}_{j,1'}^g)^2 \rangle$ . Therefore, the first term on the right hand side of eq.(15) is always  $\sim 1$ . It is irrelevant to the non-Gaussian features. The non-Gaussian signal fully comes from the second term on the right hand side of eq.(15).

If the galaxy field is Gaussian, we have

$$C_j^{2,2}(|l - l'|)_{\text{cross}} \simeq \begin{cases} 1 + 3f^2 \simeq 1.03 & |l - l'| = 0 \\ 1 & |l - l'| > 0 \end{cases} \quad (16)$$

where we used  $f = 0.1$ . Thus, we may expect that the non-Gaussian kurtosis of 2MASS galaxies shown in Figure 5 will induce  $C_j^{2,2}(0)_{\text{cross}} > 1.03$ .

The cross-correlation  $C_j^{2,2}(|l - l'|)_{\text{cross}}$  for the WMAP map and 500 2MASS DWT clusters is shown in Fig. 6. In the top panel of Fig.6, the solid and dotted line are for  $W$  and  $Q$  band respectively. The black points and error bars are the mean and 90% range of 100 simulation samples without SZ term. Therefore, Fig. 6 do show  $C_j^{2,2}(0)_{\text{cross}} > 1.03$ . The middle and bottom panels of Fig. 6 are, respectively, the  $C_j^{2,2}(|l - l'|)_{\text{cross}}$  vs.  $|l - l'|$  for mock sample A and B with  $f = 0.1$ . The error bars are the 90% range of 100 mock samples. From Fig. 6, one can conclude that 1.) There are positive signals of the  $4^{\text{th}}$  cross correlation between the wavelet variables of WMAP data and 2MASS clusters; 2.) The  $4^{\text{th}}$  cross-correlation is consistent with the estimation of mock samples A and B, and therefore, this non-Gaussian feature probably is from the SZ effect of 2MASS galaxies.

#### 4.3 Cross-correlation vs. auto-correlation

The last problem we should study is whether the SZ-effect caused non-Gaussianity can also be seen with the high order auto-correlations of WMAP maps. This point can be analyzed with the  $4^{\text{th}}$  order detector defined as

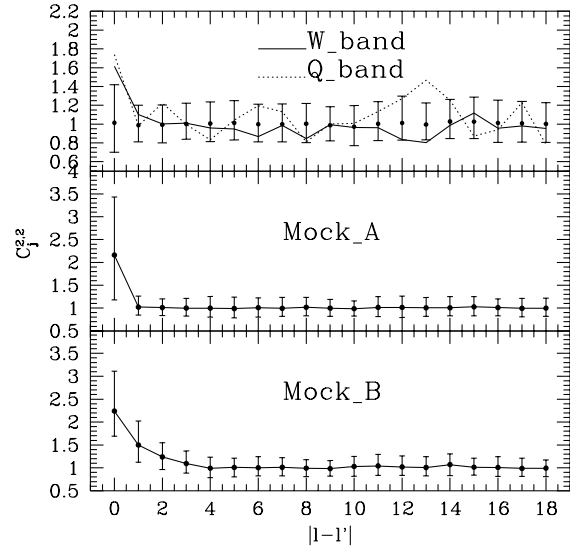


**Figure 6.**  $C_j^{2,2}(|l - l'|)_{\text{cross}}$  between a.) (top) WMAP map and top 500 2MASS DWT clusters on scale  $j = 8$ , in which solid and dotted line are for  $W$  and  $Q$  band respectively, and the black points and error bars are the mean and 90% range of 100 simulation samples without SZ term; b.) (middle) the mock sample A and top 500 2MASS DWT clusters on scale  $j = 8$ ; c.) (bottom) the mock sample B and top 500 2MASS DWT clusters on scale  $j = 8$ . The error bars of b.) and c.) are the 90% range of 100 mock samples

$$C_j^{2,2}(|l - l'|)_{\text{cmb}} = \frac{\langle (\tilde{\epsilon}_{j,1}^T)^2 (\tilde{\epsilon}_{j,1'}^T)^2 \rangle}{\langle (\tilde{\epsilon}_{j,1}^T)^2 \rangle \langle (\tilde{\epsilon}_{j,1'}^T)^2 \rangle}. \quad (17)$$

This detector actually is similar to  $C_j^{2,2}(|l - l'|)_{\text{cross}}$  [eq.(14)], but instead of  $\tilde{\epsilon}_{j,1}^g$  by  $\tilde{\epsilon}_{j,1}^T$ .

Using eqs.(9) and (10), we have

$$C_j^{2,2}(|l - l'|)_{\text{cmb}} = \begin{aligned} & \text{terms irrelevant to nongaussianity} \\ & + f^4 \frac{\langle (\tilde{\epsilon}_{j,1}^{g\alpha})^2 (\tilde{\epsilon}_{j,1'}^{g\alpha})^2 \rangle}{\langle (\tilde{\epsilon}_{j,1}^{g\alpha})^2 \rangle \langle (\tilde{\epsilon}_{j,1'}^{g\alpha})^2 \rangle}. \end{aligned} \quad (18)$$

Comparing eq.(18) with eq.(15), it is clear that the non-Gaussian term in eq.(15) is proportional to  $f^2$ , while in eq.(18) to  $f^4$ . Therefore, the SZ signal in  $C_j^{2,2}(|l - l'|)_{\text{cmb}}$  is weaker than that in  $C_j^{2,2}(|l - l'|)_{\text{cross}}$  by a factor  $f^2$ , which can be as small as  $\simeq 10^{-2}$  if considering mock samples A and B. Thus, it is not surprised that this non-Gaussianity is undetectable with current CMB maps like WMAP.

Figure 7 gives  $C_j^{2,2}(|l - l'|)_{\text{cmb}}$  vs.  $|l - l'|$  for  $W$  and  $Q$  bands of WMAP data, and for mock samples A and B. It shows no significant non-Gaussianity. Therefore, the detector of cross correlation  $C_j^{2,2}(|l - l'|)_{\text{cross}}$  is effective to pick up the SZ-effect-induced non-Gaussianity, while the detector of auto-correlation  $C_j^{2,2}(|l - l'|)_{\text{cmb}}$  is not sensitive to that non-Gaussianity. This result is not limited with the  $4^{\text{th}}$  order detectors, but it should be a common feature of high order detectors eq.(12). To replace  $(\tilde{\epsilon}_{j,1}^g)^2$  with  $(\tilde{\epsilon}_{j,1}^T)^2$  will lead to a factor  $f^2$  in the non-Gaussian term, and therefore, the cross-correlation detectors generally are more sensitive to the SZ-effect induced non-Gaussianity than auto-correlation of CMB maps.

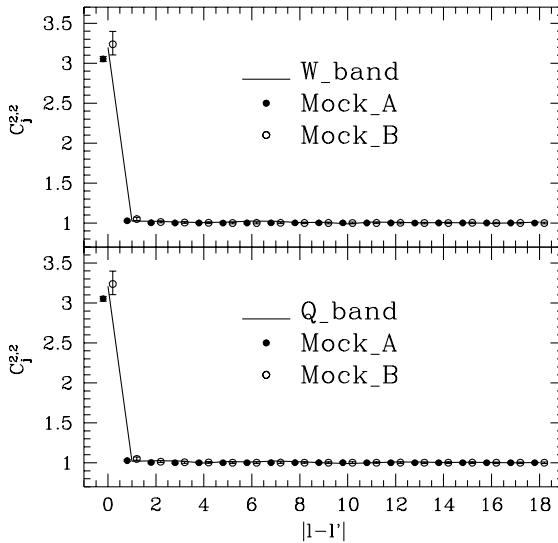


**Figure 7.**  $C_j^{2,2}(|l - l'|)_{cmb}$  vs.  $|l - l'|$  for  $W$  (top) and  $Q$  (bottom) bands of WMAP data. The mock samples of A and B are also shown. The error bars are the 90% range of 100 simulation samples.

## 5 CONCLUSION

With the DWT clusters of 2MASS sample, we confirmed the previous results of the SZ effect of 2MASS galaxies on the WMAP data (Myers et al. 2004; Afshordi et al. 2004). For the foreground cleaned WMAP maps of  $W$  and  $Q$  bands, there are about 0.4-1% area of the maps is contaminated by the SZ effect of 2MASS DWT clusters with the Compton parameter  $y = (3.7 \pm 2.4) \times 10^{-6}$ . With mock samples of the 2MASS SZ effect, we show that the non-Gaussianity of the 2MASS galaxies is imprinted on WMAP maps. This non-Gaussianity can be seen with the 4<sup>th</sup> order cross correlation between the wavelet variables of the maps of the WMAP data and 2MASS clusters. The intensity of the 4<sup>th</sup> order non-Gaussian features is consistent with the estimation given by the mock samples of the SZ effect of 2MASS galaxies. We show also that this non-Gaussianity can not be seen by the 4<sup>th</sup> and higher order auto-correlation of the WMAP maps.

The space-scale decomposition of the DWT is powerful tool for studying the SZ effect. The DWT variable can be applied to find clusters from galaxy samples, to identify the SZ effect of the DWT clusters, to detect the non-Gaussianity with high order correlation. With this method, all statistics are based on the same set of the DWT variables with well defined scale, position and shape of the modes, the relation between the SZ effect contamination and non-Gaussianity of the CMB maps can be measured without ambiguous parameters.

We also found, because the ratio between powers of SZ maps to the CMB maps generally is much less than 1, the cross correlation between the WMAP map and galaxy distribution would be more effective to pick up non-Gaussianity than auto-correlation of the WMAP map. Due to the limitation of the resolution of WMAP data, we studied only the SZ effect on scale  $j = 8$ , or  $\simeq 0^{\circ}.5$ . Once higher resolution map is available, the ratio  $C_j^{2,2}(|l - l'|)_{cmb}/C_j^{2,2}(|l - l'|)_{cross}$  would be able to provide more information of the ratio of the powers of SZ effect and CMB fluctuations on different scales.

## ACKNOWLEDGMENTS

We acknowledge the use of the HEALPix software and analysis package for producing simulation maps of the CMB. Liang Cao thanks Yi-Cheng Guo for his help. This work is in partial supported by the NSF AST-0507340.

## REFERENCES

Afshordi N., Loh Y.-S., & Strauss M. A. 2004, Phys. Rev. D, 69, 083524  
 Afshordi N., Lin Y.-T., & Sanderson A. J. R. 2005 ApJ, 629, 1  
 Bennett C. L., et al. 2003a, ApJ, 148, 1  
 Bennett C. L., et al. 2003b, ApJS, 148, 97  
 Böhringer, H., et al. 2000, ApJS, 129, 435  
 Cole, S., & Kaiser, N. 1988, MNRAS, 233, 637  
 Cooray, A., B. Daniel, Sigurdson, K. 2004, astro-ph/0410006  
 Cruz, M., Martinez-Gonzalez, E., Vielva, P. & Cayon, L. 2005, MNRAS, 356, 29  
 Daubechies I. 1992, Ten Lectures on Wavelets, (Philadelphia: SIAM)  
 Ebeling, H., et al. 1998, MNRAS, 301, 881E  
 Fang, L.Z., & Feng, L.L. 2000, ApJ, 539, 5  
 Guo, Y.C., Chu, Y.Q., & Fang, L.Z. 2004, ApJ, 610, 51  
 He, P., Feng, L.L., & Fang, L.Z. 2004, ApJ, 612, 14  
 He, P., Feng, L.L., & Fang, L.Z. 2005, ApJ, 623, 601  
 Hernández-Monteagudo, C. & Rubiño-Martín, J.A. 2004, MNRAS, 347, 403  
 Jarrett, T. H., Chester, T., Cutri, R., Schneider, S., Skrutskie, M., & Huchra, J. P. 2000, AJ, 119, 2498  
 Jing Y.P., & Fang L.Z. ApJ, 432, 438  
 Komatsu, et al. 2003 ApJS, 148, 119  
 Maddox, S. J.; Efstathiou, G.; Sutherland, W. J.; Loveday, J. 1990, MNRAS, 243, 692M  
 McEwen, J.D., Hobson, M.P., Lasenby, A.N., Mortlock, D.J. 2004, astro-ph/0406604  
 McIntosh, D. H., Maller, A. H., Katz, N., & Weinberg, M. D. 2003, RMxAC, 17, 183  
 Myers, A. D.; Shanks, T.; Outram, P. J.; Frith, W. J.; Wolfendale, A. W. 2004, MNRAS, 347, 67  
 Pando, J., & Fang, L.Z. 1998, A&A, 340, 335  
 Pando, J., Valls-Gabaud, D. & Fang, L.Z. 1998, Phys. Rev. Lett., 81, 4568  
 Pando, J., Feng, L.L., Jamkhekar, P., Zheng, W., Kirkman, D., Tytler, D. and Fang, L.Z. 2002, ApJ, 574, 575  
 Peebles, P. 1980, The large scale structures of the universe, (Princeton press)  
 Seljak, U. 1996, ApJ, 463, 1  
 Tuluie, R., Laguna, P., & Anninos, P. 1996, ApJ, 463, 15  
 Xu, W., Fang, L.Z., Deng, Z.G. 1999 ApJ, 524, 1  
 Xu, W., Fang, L.Z., Wu, X.P. 2000 ApJ, 508, 472

## APPENDIX A: ALGORITHM WITH THE DISCRETE WAVELET TRANSFORM (DWT)

Consider a 1-D density fluctuation  $\delta(x)$  on a spatial range from  $x = 0$  to  $L$ . We divide the space into  $2^j$  segments labelled by  $l = 0, 1, \dots, 2^j - 1$  each of size  $L/2^j$ . The index  $j$  is a positive integer and gives the length scale  $L/2^j$ . The larger the  $j$  is, the smaller the length scale. Any reference to a property as a function of scale  $j$  below must be interpreted as the property at length scale  $L/2^j$ . The index  $l$  represents position and it corresponds to the spatial range  $lL/2^j < x < (l+1)L/2^j$ . Hence, the space  $L$  is decomposed into cells  $(j, l)$ .

The discrete wavelet is constructed such that each cell  $(j, l)$  supports a compact function, the scaling function  $\phi_{j,l}(x)$ . In our calculations, the Daubechies 4 wavelet (Daubechies, 1992) are used. The scaling function satisfies the orthogonal relation

$$\int \phi_{j,l}(x)\phi_{j,l'}(x)dx = \delta_{l,l'}, \quad (\text{A1})$$

where  $\delta^K$  is Kronecker delta function. The scaling function  $\phi_{j,l}(x)$  is a window function on scale  $j$  centered at the segment  $l$ . The normalization of the scaling function is  $\int \phi_{j,l}(x)dx = (L/2^j)^{1/2}$ .

For a field  $\rho(x)$ , its mean in cell  $(j, l)$  can be estimated by

$$\rho_{j,l} = \frac{\epsilon_{j,l}^\rho}{\int_0^L \phi_{j,l}(x)dx}, \quad (\text{A2})$$

where  $\epsilon_{j,l}^\rho$  is called scaling function coefficient (SFC), given by

$$\epsilon_{j,l}^\rho = \int_0^L \rho(x)\phi_{j,l}(x)dx. \quad (\text{A3})$$

A 1-D field  $\rho(x)$  can be decomposed into

$$\rho(x) = \sum_{l=0}^{2^j-1} \epsilon_{j,l}^\rho \phi_{j,l}(x) + O(\geq j). \quad (\text{A4})$$

The term  $O(\geq j)$  in eq.(A3) contains only the fluctuations of the field  $\rho(x)$  on scales equal to and less than  $L/2^j$ . This term does not have any contribution to the window sampling on scale  $j$ .

The fluctuation on scale  $j$  in cell  $(j, l)$  is given by the WFC defined as

$$\tilde{\epsilon}_{j,l}^\rho = \int_0^L \rho(x)\psi_{j,l}(x)dx. \quad (\text{A5})$$

The wavelet  $\psi_{j,l}(x)$  are orthogonal with respect to  $j$  and  $l$

$$\int \psi_{j,l}(x)\psi_{j',l'}(x)dx = \delta_{l,l'}^K \delta_{j,j'}, \quad (\text{A6})$$

They are also orthogonal with  $\phi_{j,l}(x)$  as

$$\int \phi_{j',l'}(x)\psi_{j,l}(x)dx = 0 \quad \text{if} \quad j' \leq j. \quad (\text{A7})$$

The orthonormality eq. (A1) insures that the set of  $\rho_{j,l}$  or  $\epsilon_{j,l}^\rho$  do not cause false correlations. When the “fair sample hypothesis” (Peebles 1980) holds, the average over the ensemble of the random field can be estimated by the average over modes  $(j, l)$ .

## APPENDIX B: LAMBERT PROJECTION AND GAUSSIAN FIELD

### B1 White power spectrum

For a field on spherical surface  $T(\theta, \phi)$ , we have

$$T(\Omega) = \sum_{lm} a_{lm} Y_{lm}(\Omega), \quad (\text{B1})$$

where  $Y_{lm}(\Omega)$  is spherical harmonic function. The coefficients  $a_{lm}$  are given by

$$a_{lm} = \int_{4\pi} T(\Omega) Y_{lm}(\Omega) d\Omega, \quad (\text{B2})$$

where  $d\Omega = \sin \theta d\theta d\phi$ . For a Gaussian field  $T(\Omega)$ , we have

$$\langle a_{lm} a_{l'm'} \rangle = a_l^2 \delta_{ll'} \delta_{mm'}, \quad (\text{B3})$$

where  $\langle \dots \rangle$  means the average over the ensemble of samples.  $\delta_{ll'}$  means no scale-scale correlations.

Consider a coordinate transfer, such as the Lambert projection eq.(3), as

$$x_1 = X_1(\Omega) = R\sqrt{2-2|\sin \theta|} \cos \phi, \quad (\text{B4})$$

$$x_2 = X_2(\Omega) = R\sqrt{2-2|\sin \theta|} \sin \phi,$$

the field  $T$  in coordinate  $(x_1, x_2)$  is then given by

$$F(x_1, x_2) = \int \delta^D[x_1 - X_1(\Omega)]\delta^D[x_2 - X_2(\Omega)]T(\Omega)d\Omega, \quad (\text{B5})$$

where  $\delta^D$  is the Dirac delta function. Thus, the wavelet coefficients of the field  $F(x_1, x_2)$  are

$$\tilde{\epsilon}_{jp} = \int F(x_1, x_2)\psi_{jp}(x_1, x_2)dx_1dx_2 \quad (\text{B6})$$

where  $\psi_{jp}(x_1, x_2)$  is 2-dimension wavelet basis on space  $(x_1, x_2)$ . (In order to avoid the confusion between the index  $l$  for wavelet and spherical harmonic, we use  $p$  for the position index of wavelet in this Appendix).

From eqs.(B5) and (B6), we have

$$\begin{aligned} \langle \tilde{\epsilon}_{jp} \tilde{\epsilon}_{j'p'} \rangle &= \left\langle \int \psi_{jp}(X_1(\Omega), X_2(\Omega)) \right. \\ &\quad \left. \psi_{j'p'}(X_1(\Omega'), X_2(\Omega')) X_2(\Omega') T(\Omega) T(\Omega') d\Omega d\Omega' \right\rangle = \\ &= \int \psi_{jp}(X_1(\Omega), X_2(\Omega)) \psi_{j'p'}(X_1(\Omega'), X_2(\Omega')) \\ &\quad \sum_{lm} \sum_{l'm'} \langle a_{lm} a_{l'm'} \rangle Y_{lm}(\Omega) Y_{l'm'}(\Omega') d\Omega d\Omega'. \end{aligned} \quad (\text{B7})$$

For a Gaussian field eq.(B3) with constant  $a_l^2$ , we have

$$\begin{aligned} \langle \tilde{\epsilon}_{jp} \tilde{\epsilon}_{j'p'} \rangle &\propto \int \psi_{jp}(X_1(\Omega), X_2(\Omega)) \\ &\quad \psi_{j'p'}(X_1(\Omega'), X_2(\Omega')) \sum_{lm} Y_{lm}(\Omega) Y_{lm}(\Omega') d\Omega d\Omega'. \end{aligned} \quad (\text{B8})$$

Considering

$$\sum_{lm} Y_{lm}(\Omega) Y_{lm}(\Omega') = \delta^D(\Omega - \Omega'), \quad (\text{B9})$$

we have then

$$\begin{aligned} \langle \tilde{\epsilon}_{jp} \tilde{\epsilon}_{j'p'} \rangle &\propto \\ &\quad \int \psi_{jp}(X_1(\Omega), X_2(\Omega)) \psi_{j'p'}(X_1(\Omega), X_2(\Omega)) d\Omega, \end{aligned} \quad (\text{B10})$$

For the equal area projection of the Lambert transform eq.(3) or eq.(B4), we have

$$d\Omega = R^{-2} dX_1 dX_2. \quad (\text{B11})$$

Thus, eq.(B10) gives

$$\begin{aligned} \langle \tilde{\epsilon}_{jp} \tilde{\epsilon}_{j'p'} \rangle &\propto \\ &\quad \int \psi_{jp}(X_1, X_2) \psi_{j'p'}(X_1, X_2) dX_1 dX_2 = \delta_{jj'} \delta_{pp'}, \end{aligned} \quad (\text{B12})$$

The last step is based on the orthogonal-normal condition of wavelet. Therefore,  $\langle \tilde{\epsilon}_{j,l} \tilde{\epsilon}_{j',l'} \rangle$  is diagonal in terms of scale index  $j$ , i.e. free from scale-scale correlation.

### B2 Non-white power spectrum

If  $\langle a_{lm} a_{l'm'} \rangle = a_l^2 \delta_{ll'} \delta_{mm'}$  and  $a_l^2$  is not constant, the covariance  $\langle \tilde{\epsilon}_{jp} \tilde{\epsilon}_{j'p'} \rangle$  will still be diagonal or quasi-diagonal with respect to

$(j, j')$ . In this case, we should consider the locality of wavelets, i.e. in the Fourier space, the wavelet  $\psi_{jl}$  is localized in the area around scale  $j$ . From eqs.(B5) and (B6) we have

$$\tilde{\epsilon}_{jp} = \int \psi_{jp}(x_1, x_2) \delta^D[x_1 - X_1(\Omega)] \delta^D[x_2 - X_2(\Omega)] T(\Omega) d\Omega dx_1 dx_2. \quad (\text{B13})$$

Using eq.(B9) and (B2), eq.(B13) yields

$$\begin{aligned} \tilde{\epsilon}_{jp} &= \int \psi_{jp}(x_1, x_2) \delta^D[x_1 - X_1(\Omega)] \delta^D[x_2 - X_2(\Omega)] T(\Omega) d\Omega dx_1 dx_2 \\ &= \sum_{l,m} a_{lm} \int \psi_{jp}(x_1, x_2) \delta^D[x_1 - X_1(\Omega)] \delta^D[x_2 - X_2(\Omega)] Y_{lm}(\Omega) d\Omega dx_1 dx_2 \\ &= \sum_{l,m} a_{lm} \tilde{\psi}_{jp}(lm) \end{aligned} \quad (\text{B14})$$

where

$$\begin{aligned} \tilde{\psi}_{jp}(lm) &= \int \psi_{jp}(x_1, x_2) \delta^D[x_1 - X_1(\Omega)] \delta^D[x_2 - X_2(\Omega)] Y_{lm}(\Omega) d\Omega dx_1 dx_2, \\ & \end{aligned} \quad (\text{B15})$$

$\tilde{\psi}_{jp}(lm)$  actually is the wavelet  $\psi_{jp}$  in the  $(lm)$ -representation. Our goal below is to show that  $\psi_{jp}(lm)$  is localized in the  $(lm)$ -space.

Using the Fourier representation of  $\delta^D$  function, we have

$$\begin{aligned} \tilde{\psi}_{jp}(lm) &= \frac{1}{4\pi^2} \int dk_1 dk_2 \\ &\quad \int \psi_{jp}(x_1, x_2) e^{i(x_1 k_1 + x_2 k_2)} dx_1 dx_2 \\ &\quad \int e^{i[X_1(\Omega) k_1 + X_2(\Omega) k_2]} Y_{lm}(\Omega) d\Omega \\ &= \frac{1}{4\pi^2} \int dk_1 dk_2 \hat{\psi}_{jp}(k_1, k_2) \int d\Omega e^{i\sqrt{2}Rk \cos \theta'} Y_{lm}(\Omega). \end{aligned} \quad (\text{B16})$$

where  $\hat{\psi}_{jl}(k_1, k_2)$  is the Fourier transform of the wavelet. In the last step of eq.(B16), we used Eq.(B4),  $k_1 = k \cos \phi$ ,  $k_2 = k \sin \phi$  (or  $k = (k_1^2 + k_2^2)^{1/2}$ ) and  $\cos \theta' \equiv \sqrt{1 - |\sin \theta|}$ . Wavelet  $\hat{\psi}_{jl}(k_1, k_2)$  is localized in  $k$ -space. For a given  $\mathbf{j} = (j_1, j_2)$ ,  $\hat{\psi}_{jl}(k_1, k_2)$  is localized in the range  $2\pi 2^{j_1-1/2}/R < k_1 < 2\pi 2^{j_1+1/2}/R$  and  $2\pi 2^{j_2-1/2}/R < k_2 < 2\pi 2^{j_2+1/2}/R$ . Therefore, for the case  $j_1 = j_2 = j$ , the wavelet  $\hat{\psi}_{jl}(k_1, k_2)$  is localized in the  $k$ -band of  $2\pi 2^j/R < k < 2\pi 2^{j+1}/R$ .

After the integral on azimuthal angle  $\phi$ , eq.(B16) gives

$$\begin{aligned} \tilde{\psi}_{jp}(lm) &= \delta_{0m} \frac{\sqrt{2l+1}}{2\pi^{3/2}} \int dk_1 dk_2 \hat{\psi}_{jp}(k_1, k_2) \\ &\quad n \int d\cos \theta e^{i\sqrt{2}Rk \cos \theta'} P_l(\cos \theta). \end{aligned} \quad (\text{B17})$$

Using the expansion of  $e^{i\sqrt{2}Rk \cos \theta'}$  with  $P_l'(\cos \theta')$ , we have

$$\begin{aligned} \tilde{\psi}_{jp}(lm) &= \delta_{0m} \frac{\sqrt{2l+1}}{2\pi^{3/2}} \sum_{l'} (2l'+1) i^{l'} \\ &\quad \int dk_1 dk_2 \hat{\psi}_{jp}(k_1, k_2) j_l(\sqrt{2}Rk) \\ &\quad \int P_{l'}(\cos \theta') P_l(\cos \theta) d\cos \theta, \end{aligned} \quad (\text{B18})$$

where  $j_l(x)$  is spherical Bessel function. First, we take approximation  $\cos \theta' \simeq \cos \theta$ , eq.(B18) gives

$$\tilde{\psi}_{jp}(lm) = \delta_{0m} \frac{\sqrt{2l+1}}{\pi^{3/2}} i^l \int dk_1 dk_2 \hat{\psi}_{jp}(k_1, k_2) j_l(\sqrt{2}Rk) \quad (\text{B19})$$

where  $j_l(x)$  is the spherical Bessel function. It is known that the function  $j_l(x) \ll 1$ , when  $x < l$ , it approaches its peak at  $x \simeq l\pi$ , and oscillating around zero when  $x > l\pi$ . On the other hand,  $\hat{\psi}_{jp}(k_1, k_2)$  is slowly varying with  $k$  in the range  $2^j/R < k/2\pi < 2^{j+1}/R$ . Therefore, the integral on  $k$  in eq.(B19) is of non-zero mainly in the range of  $l \simeq \sqrt{2}Rk/\pi$ . Thus, from the  $k$ -band of  $2\pi 2^j/R < k < 2\pi 2^{j+1}/R$ , we have that for large  $j$ ,  $\tilde{\psi}_{jp}(lm)$  is of non-zero mainly in the  $l$ -band given by

$$2^{j+3/2} < l < 2^{j+5/2}. \quad (\text{B20})$$

This result actually is the well known property of the localization of wavelet in scale space, regardless that the scale-space is described by  $k$ - or  $l$ -representations.

Now, let us consider the effect of  $\cos \theta' \neq \cos \theta$ . One can estimate this effect by the expansion  $P_{l'}(\cos \theta') = P_{l'}(\cos \theta + \eta) = P_{l'}(\cos \theta) + \sum (\eta^n/n!) P_{l'}^{(n)}(\cos \theta)$ , where  $\eta \equiv \cos \theta' - \cos \theta = \sqrt{1 - \sin \theta} - \cos \theta$ . The derivative of Legendre function,  $P_{l'}^{(n)}(\cos \theta)$ , can be expressed by a summation of  $P_{l-n} \dots P_{l+n}$ . Therefore, the  $n^{th}$  correction may enlarge the  $l$ -band from  $2^{j+3/2} - 2^{j+5/2}$  to  $(2^{j+3/2} - n) - (2^{j+5/2} + n)$ . Since  $\eta < 0.3$ , we need to consider only a few low order corrections, say  $n \leq 3$ . On the other hand, for high  $j$  (small scales) case, we have  $2^j \gg 1$ , or  $2^j \gg n$ , and therefore, the  $\eta$  correction on the  $l$ -band of  $\tilde{\psi}_{jp}(lm)$  is small when  $j$  is large.

One can then conclude that, for different  $j$ , the wavelet  $\tilde{\psi}_{jp}(lm)$  consists of  $a_{jm}$  in different  $l$ -band, or the  $l$ -bands for  $j$  and  $j'$  ( $j \neq j'$ ) basically are not overlapped. From eq.(B14), the coefficients  $a_{lm}$  in different  $l$ -bands are uncorrelated. Thus, the covariance  $\langle \tilde{\epsilon}_{jp} \tilde{\epsilon}_{j'p'} \rangle$  should be diagonal or quasi-diagonal as

$$\langle \tilde{\epsilon}_{jp} \tilde{\epsilon}_{j'p'} \rangle \simeq 0, \quad \text{if } j \neq j'. \quad (\text{B21})$$